Improved Spectrum Width Estimators for Doppler Weather Radars

David (left), Sebastián (right)

David A. Warde[1,2] and Sebastián M. Torres[1,2]

[1]*Cooperative Institute for Mesoscale Meteorological Studies, The University of Oklahoma, and* [2]*NOAA/OAR National Severe Storms Laboratory, Norman, Oklahoma, United States of America,*

(Dated: 30 June 2014)

Abstract

On Doppler weather radars, the spectrum width is commonly estimated from a ratio of autocorrelation estimates at two different lags. These estimators, referred to as pulse-pair processing (PPP), perform better and are computationally less expensive than frequency-domain estimators based on the Doppler spectrum. PPP estimators have been used for decades on operational weather radars and have well known properties. For example, out of all PPP estimators, the R0/R1 estimator, which is based on the ratio of lag-0 to lag-1 autocorrelations, performs the best for wide spectrum widths but has poor performance for narrow spectrum widths and relies on accurate noise measurements. The R1/R2, which is based on the ratio of lag-1 to lag-2 autocorrelations, and other estimators based on higher-lag autocorrelations provide better narrow spectrum-width estimates than the R0/R1 estimator and improve performance when accurate noise measurements are not available, but they are severely biased for wide spectrum widths. Thus, to provide better estimates over a wide range of spectrum widths, a few PPP estimators can be suitably combined. This so-called hybrid spectrum-width estimator can take advantage of the best characteristics of each estimator for different regimes. However, the performance of all PPP estimators degrades when the number of samples is small. This degradation is evident as a higher number of invalid estimates (negative spectrum widths) and increased biases and variances for narrow spectrum widths. In this work, we propose a new class of PPP spectrum-width estimators that are based on "matched" autocorrelation ratios. Autocorrelation estimators are said to be "matched" if they use the time-series samples in the same manner. When compared to conventional PPP estimators, the proposed estimators exhibit improved performance for small numbers of samples. This is quantified and illustrated using simulations and real data collected with operational WSR-88D radars.

1. Introduction

A category of spectrum width estimators used for Doppler weather radar which rely on a Gaussian shaped power spectrum are of the form

$$\hat{\sigma}_v(m,m') = \frac{v_a\sqrt{2}}{\pi\sqrt{(m'^2-m^2)}}\left|\ln\left(\frac{\left|\hat{R}(mT_s)\right|-\delta_{m,0}N}{\left|\hat{R}(m'T_s)\right|}\right)\right|^{1/2}, \quad (1)$$

where v_a is the unambiguous velocity, $\hat{R}(mT_s)$ is the autocorrelation at lag m with pulse repetition time (PRT) T_s, $\delta_{m,0}$ is the Kronecker delta, and $m' > m$. These estimators are well documented and have known characteristics (see [1] – [17]). For instance, the $\hat{\sigma}_v(0, 1)$ estimator (often referred to as the R0/R1 estimator) provides the best wide spectrum width estimates with the lowest variance over the widest range of spectrum widths, but provides poor narrow spectrum width estimates. Whereas the use of higher lags in (1) (i.e., $m' > 1$) provide better narrow spectrum width estimates with lower variance compared with estimators using lower lags, these estimators saturate quickly for wide spectrum widths. Further, the use of higher lags for m (i.e., $m > 0$) in (1) are justified when the system noise power cannot be adequately determined despite the fact that these estimators saturate less gracefully than the estimators that use $\hat{R}(0)$ with an accurate system noise. From (1), it is easy to see that changes in the PRT have a similar effect on the performance of the estimators as do changes in the lag (i.e., larger PRTs provide better narrow spectrum widths and smaller PRTs provide better wide spectrum widths). For these estimators, the quality of the estimates degrades rapidly at low signal–to-noise ratios. Further, the performance of these estimators depends on sample size; performing better as the number of samples increases. In practice, only the first few lags are used in these estimators.

To provide better estimates over a wide range of spectrum widths, the results of several estimators can be combined to take advantage of the best characteristics of each estimator. These estimators are referred to as hybrid spectrum width estimators. As an example, a hybrid spectrum width estimator has been implemented on the NEXRAD system that uses $\hat{\sigma}_v(0, 1)$ for wide spectrum widths, $\hat{\sigma}_v(1, 2)$ for medium spectrum widths, and $\hat{\sigma}_v(1, 3)$ for very narrow spectrum widths [18]. Whereas hybrid spectrum width estimators exhibit an improved overall performance, this improvement is limited to the performance of the individual estimators available for selection. In this work we propose a new

set of spectrum width estimates based on "matched" autocorrelation estimates that exhibit improved performance over the classical estimators in (1). Thus, when combined in a hybrid approach, they result in even greater improvement to spectrum width estimation for weather radars

2. "Matched" Autocorrelations

As mentioned before, classical spectrum width estimators are based on ratios of the autocorrelation function at different lags. Thus, their performance depends not only on the individual autocorrelation estimator but also on how the time-series data is used in both autocorrelation estimators. We have found that the performance of the classical spectrum width estimators improves when the autocorrelation estimators in the ratio are "matched"; i.e., when both estimators use the time-series data with the same frequency and weights.

Autocorrelation estimators based on the Autocorrelation Spectral Density (ASD) [19] are naturally "matched". For example, the lag-1 ASD estimator is formed by combining two complex spectra F_0 and F_1 {see (2.1) and (2.2) of [19]}, and the Power Spectral Density (PSD) can be obtained from the same complex spectra as the average of their magnitudes squared [20]. Note that both spectral densities have the same frequency resolution (i.e., they are "matched"). It can be shown that the sums of the coefficients of two spectral densities provide "matched" autocorrelation estimates for lags 1 and 0, respectively. Fig. 1 illustrates this process. That is, the lag-1 ASD, $S_1(k)$, and its "matched" time-averaged modified periodogram, $S_0^1(k)$, are both formed by combining two complex spectra F_0 and F_1 (2).

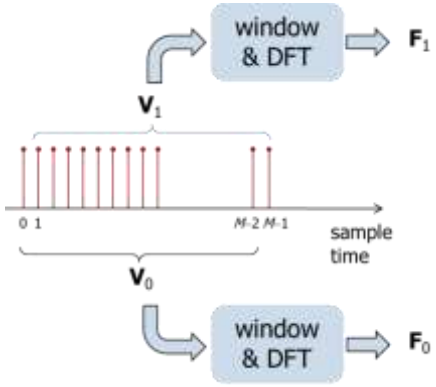

Fig. 1. Time series of M complex received voltages are divided into two $(M-1)$ subsamples: V_0 and V_1. A data window is applied and the discrete Fourier transform (DFT) is taken to create F_0 and F_1, respectively.

$$S_1(k) = F_0^*(k)F_1(k)$$
$$S_0^1(k) = \frac{|F_0(k)|^2 + |F_1(k)|^2}{2} \tag{2}$$

In the following equation, the lag-l autocorrelations and their "matched" lag-0 autocorrelations are given explicitly to show that the complex voltages (V) comprising the autocorrelation pairs are used with the same frequency and weighting.

Lag-l	"Matched" Lag-0
$\hat{R}(1) = \sum_{k=0}^{M-2} S_1(k) = \frac{1}{M-1}\sum_{l=0}^{M-2} d^*(l)V^*(l)d(l)V(l+1)$	$\hat{R}^1(0) = \sum_{k=0}^{M-2} S_0^1(k) = \frac{1}{2(M-1)}\sum_{l=0}^{M-2} \lvert d(l)V(l)\rvert^2 + \lvert d(l)V(l+1)\rvert^2$
$\hat{R}(2) = \sum_{k=0}^{M-3} S_2(k) = \frac{1}{M-2}\sum_{l=0}^{M-3} d^*(l)V^*(l)d(l)V(l+2)$	$\hat{R}^2(0) = \sum_{k=0}^{M-3} S_0^2(k) = \frac{1}{2(M-2)}\sum_{l=0}^{M-3} \lvert d(l)V(l)\rvert^2 + \lvert d(l)V(l+2)\rvert^2$
$\hat{R}(3) = \sum_{k=0}^{M-4} S_3(k) = \frac{1}{M-3}\sum_{l=0}^{M-4} d^*(l)V^*(l)d(l)V(l+3)$	$\hat{R}^3(0) = \sum_{k=0}^{M-4} S_0^3(k) = \frac{1}{2(M-3)}\sum_{l=0}^{M-4} \lvert d(l)V(l)\rvert^2 + \lvert d(l)V(l+3)\rvert^2$
⋮	⋮

(3)

3. Proposed Spectrum Width Estimators and Comparisons

The proposed spectrum width estimators are realized by using "matched" autocorrelation estimates in (1). As examples of performance, we compare standard spectrum width estimators (1) used in the WSR-88D, $\hat{\sigma}_v(0, 1)$, $\hat{\sigma}_v(1, 2)$, and $\hat{\sigma}_v(1, 3)$ to the proposed estimators, $\hat{\sigma}_v(0^1, 1)$, $\hat{\sigma}_v(0^2, 2)$, and $\hat{\sigma}_v(0^3, 3)$ using "matched" autocorrelations (where the superscript of 0^l indicates the "matched" autocorrelations to the lag-l autocorrelation). For these comparisons a 20 dB signal-to-noise (SNR) simulated weather signal with 64 samples is used for 5 velocities spanning the Nyquist interval from 0 to 26.3 m s^{-1} with 1000 realizations at each true spectrum width of 0.1 to 15 m s^{-1}. A 2-D histogram displays the results in a logarithmic color scale as a percentage of the total realizations (5,000) from 0% (blue) to 100% (maroon). The x-axis is the true spectrum width and the y-axis is the estimated spectrum width.

Shown in Fig. 2 is the comparison of the standard estimator, $\hat{\sigma}_v(0, 1)$ (left), to proposed estimator, $\hat{\sigma}_v(0^1, 1)$ (right). A common occurrence for (1) is that a meaningless value is obtained when the magnitude of the numerator is smaller than the magnitude in the denominator. In this case, the output of the estimator is assigned a 0 m s^{-1} value. When comparing the standard (large red arrow in left image) to the proposed (large green arrow in right image) estimator at narrow spectrum widths, it is seen that the standard estimator has more occurrence of 0 m s^{-1} values than does the proposed estimator. Additionally, the standard estimator has a larger dispersion of estimates (small red arrows in left image) than does the proposed estimator (small green arrows in right image). This is evident in the lower colors of yellow and orange in the left image as compared to the concentration of reds along the 0-bias line in the right image where true and estimated spectrum widths are equal. At larger spectrum width values, the standard estimator and the proposed estimator perform similarly.

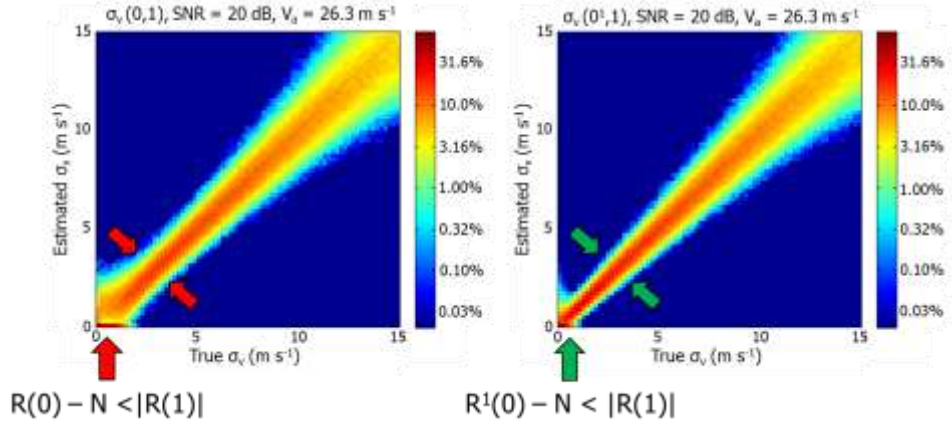

Fig. 2. 2-D histograms of true (x-axis) to estimated [y-axis, $\hat{\sigma}_v(0, 1)$ (left) to $\hat{\sigma}_v(0^1, 1)$ (right)] spectrum width for 5,000 realizations of a 20 dB SNR simulated weather signal. The logarithmic color scale displays the percentage of the total realizations (5,000) from 0% (blue) to 100% (maroon). The large arrows (bottom of figures) indicate a breakdown in the estimator where meaningless values are assigned 0 m s^{-1}. The smaller arrows indicate the spread (variance) of the output estimates.

Shown in Fig. 3 is the comparison of the standard estimator, $\hat{\sigma}_v(1, 2)$ (left), to proposed estimator, $\hat{\sigma}_v(0^2, 2)$ (right). Similar to the comparisons in Fig. 2, narrow spectrum widths biases (large red arrow in left image) and increased variance (small red arrows in left image) are seen in the standard estimator as compared to the proposed estimator (like green arrows in right image). An additional anomaly is revealed when using autocorrelation lags higher than lag-0 in the numerator of (1): the estimator provides narrow spectrum width outputs for large true spectrum widths inputs. This is seen in the standard estimator for true spectrum width values above ~7 m s^{-1} with corresponding output values as low as 0 m s^{-1}. In this case, we will say that the standard estimator saturates poorly and the proposed estimator is seen to saturate more gracefully.

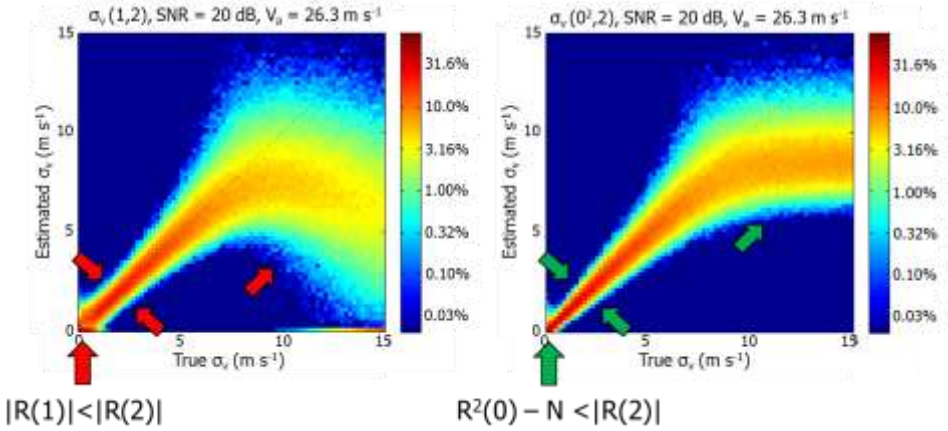

Fig. 3. Same as Fig. 2 except comparing $\hat{\sigma}_v(1, 2)$ (left) to $\hat{\sigma}_v(0^2, 2)$ (right). Additional to the large arrows (bottom of figures) that indicate a breakdown in the estimator and the smaller arrows (pointing toward each other) that indicate the spread (variance) of the output estimates, another small arrow (right of center) is added to indicate the saturation effects of the estimators.

Shown in Fig. 4 is the comparison of the standard estimator, $\hat{\sigma}_v(1, 3)$ (left), to proposed estimator, $\hat{\sigma}_v(0^3, 3)$ (right). Similar to the comparisons in Fig. 3, narrow spectrum widths biases (large red arrow in left image), increased variance (small red arrows in left image), and poor saturation effects (small red arrow right of center) are seen in the standard estimator as compared to the proposed estimator (like green arrows in right image).

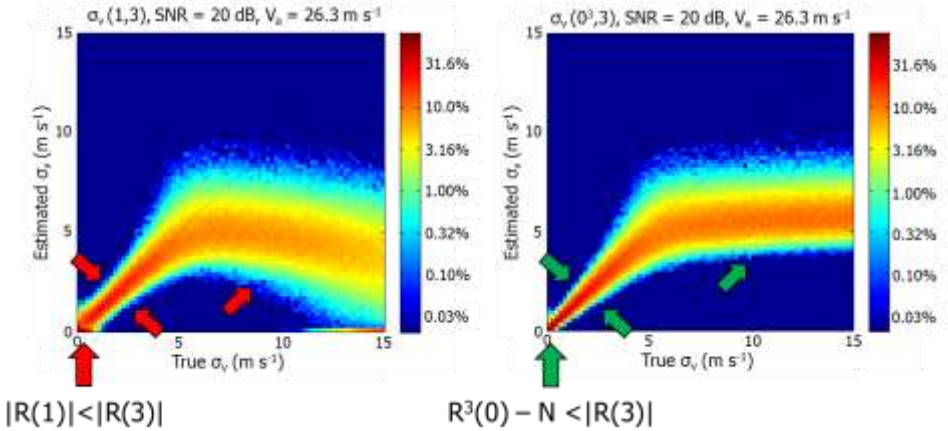

Fig. 4. Same as Fig. 3 except comparing $\hat{\sigma}_v$ (1, 3) (left) to $\hat{\sigma}_v$ (0^3, 3) (right).

4. **Application to WSR-88D Data**

4.1 Comparison of estimators

The performance of the proposed spectrum width estimators can be seen in comparison to the standard spectrum width estimators by processing unfiltered data collected from an operational WSR-88D radar. For this example, data collected on March 18, 2008 with a standard volume coverage pattern (VCP) 12 at an elevation angle of 0.5°; 16 samples per dwell at a PRT of 3.107 ms were processed for unfiltered reflectivity estimates, and 44 samples per dwell at a PRT of 0.987 ms (v_a = 26.1 m s^{-1}) were processed (independently) for unfiltered Doppler velocity and spectrum width estimates. In Fig. 5, unfiltered reflectivity (left) and velocity (right) plan-position-indicator (PPI) displays show stratiform rain north of the radar.

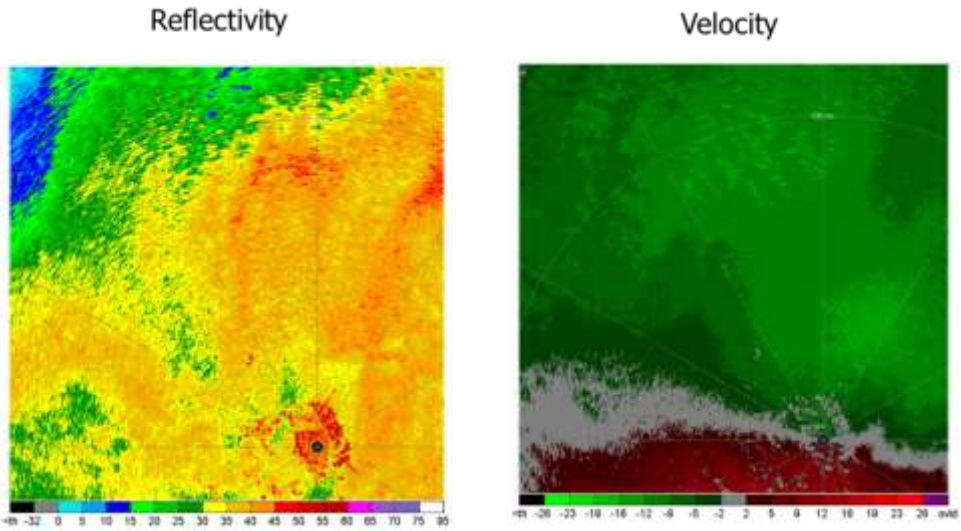

Fig. 5. Reflectivity (left) and velocity (right) PPI displays from WSR-88D radar on March 18, 2008.

In Fig. 6, PPI displays of the $\hat{\sigma}_v(0, 1)$ (left) and $\hat{\sigma}_v(0^1, 1)$ (right) are shown. The color scale has been altered to display blue for spectrum width estimates of 0 m s^{-1} to highlight those regions where meaningless values occur. In this case, the standard estimator on the left shows more zero values than does the proposed estimator on the right. Additionally, both estimators perform similarly for wide spectrum widths as seen in the upper and lower portions of the displays. Recall from the introduction that for wide spectrum width values, these estimators are the best. Although difficult to establish from the images, the proposed estimator seems to have less bias and appears smoother for narrow spectrum width values. The performance of these estimators is as expected from the discussion related to the simulation results in Fig. 2. Narrow spectrum width recovery is even better in Fig. 7 where PPI displays of the $\hat{\sigma}_v(1, 2)$ (left) and $\hat{\sigma}_v(0^2, 2)$ (right) are shown; however, note that the wide spectrum width values are not properly represented by either estimator as seen by comparing the high spectrum width regions along the top and bottom of the PPI displays in Fig.6 to those in Fig. 7 where lower values are observed for the same regions. Even so, the standard estimator is seen to produce near-zero values for very high spectrum widths due to the estimators saturation effects. The best narrow spectrum width values of those tested come from the estimators in Fig. 8, where PPI displays of the $\hat{\sigma}_v(1, 3)$ (left) and $\hat{\sigma}_v(0^3, 3)$ (right) are shown; however, note that there are less high spectrum width values than previously seen in Fig. 6. That is, both estimators provide biased high spectrum width estimates as expected from the analysis of these estimators in 3 (see Fig. 4). Still, improvements in narrow spectrum width recovery are better in the proposed estimator.

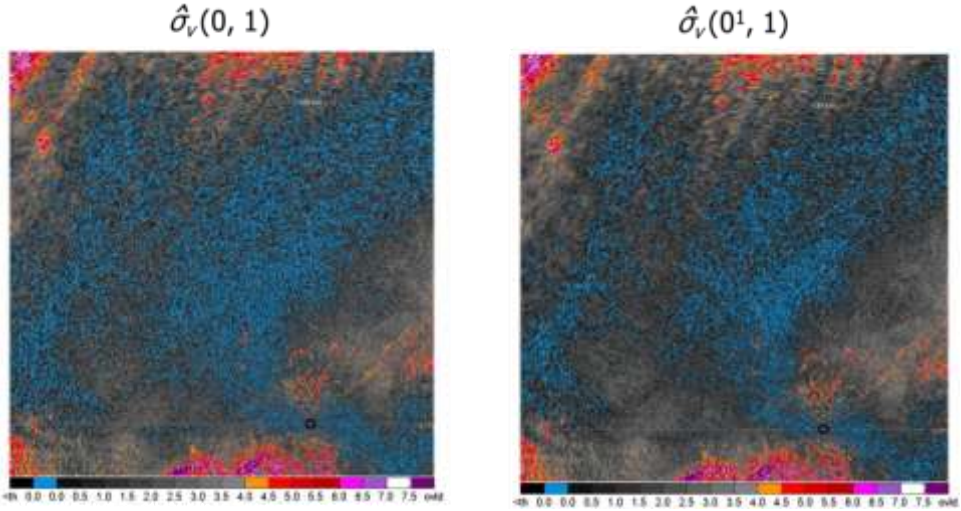

Fig. 6. Spectrum width PPI displays of $\hat{\sigma}_v(0, 1)$ (left) and $\hat{\sigma}_v(0^1, 1)$ (right). The blue color is where the estimate output is set to 0 m s^{-1}.

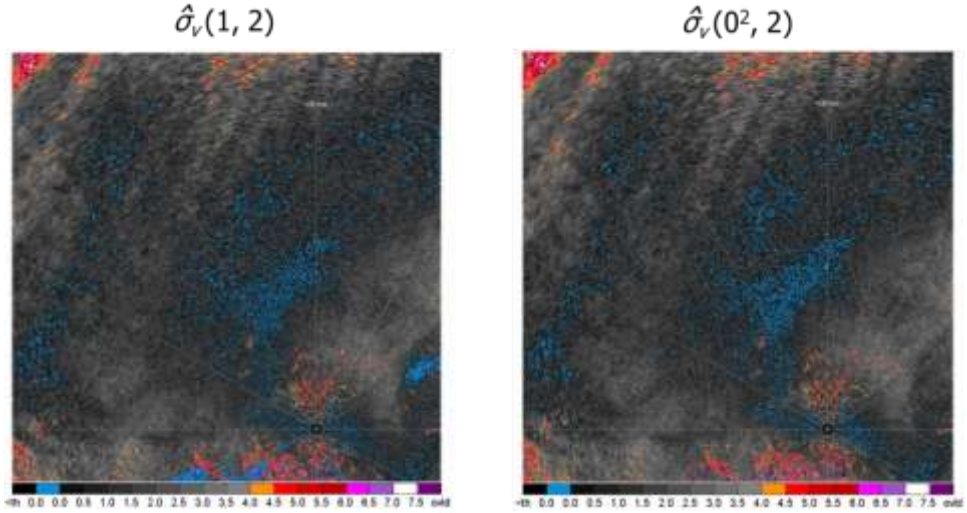

Fig. 7. Same as Fig. 6 except spectrum width PPI displays of $\hat{\sigma}_v(1, 2)$ (left) and $\hat{\sigma}_v(0^2, 2)$ (right).

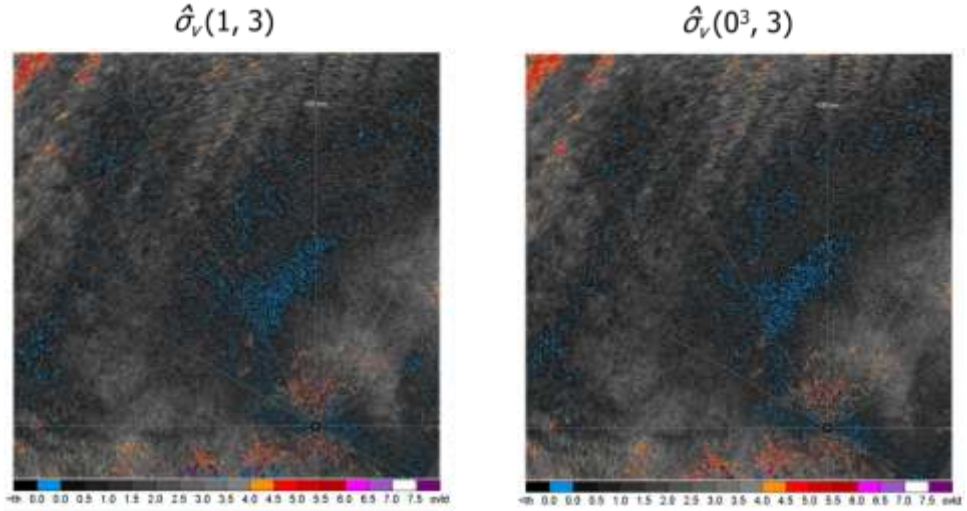

Fig. 8. Same as Fig. 6 except spectrum width PPI displays of $\hat{\sigma}_v(1, 3)$ (left) and $\hat{\sigma}_v(0^3, 3)$ (right).

4.2 A Simple Hybrid Spectrum Width Estimator

As mentioned before, a hybrid approach to spectrum width estimation uses the best characteristics of each individual estimator. In general, to measure wide spectrum widths, the $\hat{\sigma}_v(0, 1)$ and $\hat{\sigma}_v(0^1, 1)$ estimators perform the best; and, the use of higher autocorrelation lags in the denominator in (1) allows for better narrow spectrum width recovery. This can be readily seen by examining the Gaussian autocorrelation function which is typical of weather signals for both wide and narrow spectrum widths. For wide spectrum widths, the ACF is narrow and the magnitude falls off rapidly after a few lags; whereas, for narrow spectrum widths, the ACF is wide and longer lags are needed to get an appreciable change in magnitude. For the WSR-88D, a hybrid spectrum width estimator uses $\hat{\sigma}_v(0, 1)$ for wide, $\hat{\sigma}_v(1, 2)$ for medium, and $\hat{\sigma}_v(1, 3)$ for narrow spectrum width recovery. The choice of which estimator to use is based on fuzzy logic [18]. A simple hybrid spectrum width estimator can also be created using the proposed estimators: $\hat{\sigma}_v(0^1, 1)$, $\hat{\sigma}_v(0^2, 2)$, and $\hat{\sigma}_v(0^3, 3)$. In this simple approach, we choose the estimator that has the best performance for wide spectrum widths, $\hat{\sigma}_v(0^1, 1)$, as long as it does not provide a meaningless value, which is more likely as the spectrum width becomes narrower. If a meaningless value occurs, we choose the next best "wide" spectrum width estimator, $\hat{\sigma}_v(0^2, 2)$. Lastly, if the $\hat{\sigma}_v(0^2, 2)$ produces a meaningless value, we choose $\hat{\sigma}_v(0^3, 3)$.

Next, we apply our new estimator to the same data as in 4.1. In Fig. 9, the WSR-88D hybrid spectrum width estimator (left) and a simple hybrid spectrum width estimate (right) is shown. Both estimators provide good wide spectrum estimates; however, the WSR-88D hybrid spectrum width estimator shows some narrow spectrum width values that should be wider (top-left and bottom-right in display). The bias is observed when comparing regions of high spectrum width estimates in Fig. 6 (left display) to like regions in Fig. 9 (left display) and recalling

that the estimator in Fig. 6 (left display) should provide the best possible wide spectrum width estimates of the available estimates to the WSR-88D hybrid spectrum width estimator. These same high spectrum width regions appear to be displayed properly by the simple hybrid spectrum width estimator (compare Fig. 6 and Fig. 9 right displays). Additionally, the simple approach appears to have fewer zeroes than does the WSR-88D hybrid spectrum width estimator. This is because the fuzzy logic in the latter only chooses between the $\hat{\sigma}_v(0, 1)$ and $\hat{\sigma}_v(1, 2)$ for this case. That is, the $\hat{\sigma}_v(1, 3)$ is not used at all. Still, it is difficult to establish which estimator provides the best narrow spectrum width values and further analysis is needed.

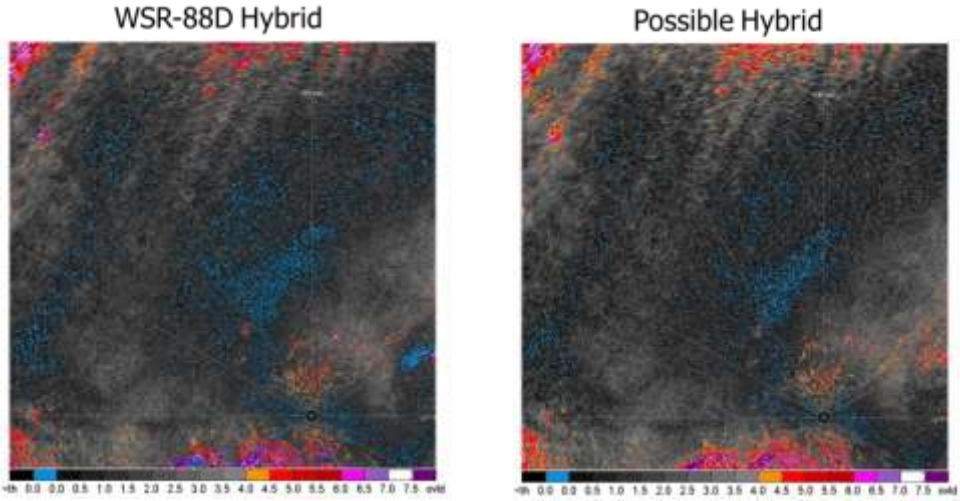

Fig. 9. Same as Fig. 6 except spectrum width PPI displays of WSR-88D (left) and proposed (right) hybrid spectrum width estimators.

5. Conclusions

This paper introduced the concept of "matched" autocorrelation estimates to produce improved spectrum width estimators. When compared to conventional PPP estimators, the proposed estimators exhibit improved performance in terms of bias and standard deviation for narrow spectrum widths, and saturation characteristics for wide spectrum widths. This was illustrated through simulations and real data collected on a WSR-88D radar. In general, it was seen that the best wide spectrum with estimator uses the lowest possible lags; whereas the best narrow spectrum width estimator uses larger autocorrelation lags. Combining the best characteristics of the proposed estimators into a simple hybrid spectrum width estimator highlighted the advantages of the hybrid approach as well as the improved performance of the new estimators. Although the results are promising, a complete characterization of the new estimators is warranted. For example, performance at low SNR, different samples sizes, and different PRTs are needed to develop an optimal hybrid spectrum width estimator.

6. Acknowledgment

This conference paper was prepared by David Warde and Sebastián Torres with funding provided by NOAA/Office of Oceanic and Atmospheric Research under NOAA-University of Oklahoma Cooperative Agreement #NA11OAR4320072, U.S. Department of Commerce. The statements, findings, conclusions, and recommendations are those of the authors and do not necessarily reflect the views of NOAA or the U.S. Department of Commerce.

REFERENCES

[1] Benham, F. C., H. L. Groginsky, A. S. Soltes, and F. Works, 1972: "Pulse Pair Estimation of Doppler Spectrum Parameters," Final report, Contract F-19628-71-C-0126", Raytheon Co., EDL, Wayland, MA, 157 pp.

[2] Berger, T. and H. L. Groginsky, 1973: "Estimation of the spectral moments of pulse trains." Int. Conf. on Inform. Theory, Tel Aviv, Israel, 30 pp.

[3] Bringi, V. N., and V. Chandrasekar, 2001: *Polarimetric Doppler Weather Radar: Principles and Applications*. Cambridge University Press, 636 pp.

[4] Doviak, D. and D. Zrinć: 1993, *Doppler Radar and Weather Observations*, 2nd ed. Academic Press. 562 pp.

[5] Melnikov, V. M., and D. S. Zrnić, 2004: Estimates of large width from autocovariances. *J. Atmos. Oceanic Technol.*, vol. **21**, 969–974.

[6] Miller, K. S., and M. M. Rochwarger, 1972: A covariance approach to spectral moment estimation, *IEEE Trans. Inform. Theory*, vol. **IT-18**, 588–596.

[7] Novak, L. M., 1983: "On the estimation of spectral parameters using burst waveforms." Massachusetts Institute of Technology Lincoln Labs Tech. Report 672, Lexington, MA, 59 pp.

[8] Rummler, W. D., 1968a: "A statistical model for scattering from a range cell of the wake." Tech. Memo. MM-68-4121-11, Bell Telephone Labs, Whippany, NJ, 21 pp.

[9] ___, 1968b: "Two pulse spectral measurements." Tech. Memo. MM-68-4121-15, Bell Telephone Labs, Whippany, NJ, 20 pp.

[10] Srivastava, R. C., A. R. Jameson, and P. H. Hildebrand, 1979: Time-domain computation of mean and variance of Doppler spectra. *J. Appl. Meteor.*, vol. **18**, 189–194.

[11] Zrnić, D. S., 1975a: Moments of estimated input power for finite sample averages of radar receiver outputs. *IEEE Trans. Aerosp. Electron. Syst.*, vol. **AES-11**, 109–113.

[12] ___, 1975b: Simulation of weather like Doppler spectrum and signals, *J. of Applied Meteorology*, vol. **14**, 619–620.

[13] ___, 1977: Spectral moment estimates from correlated pulse pairs. *IEEE Trans. Aerosp. Electron*. Syst., vol. **AES-13**, 344–354.

[14] ___, 1979a: Estimation of spectral moments for weather echoes. *IEEE Trans. Geosci. Electron.*, vol. **GE-17**, 113–128.

[15] ___, 1979b: Spectrum width estimates for weather echoes. *IEEE Trans. Aerosp. Electron. Syst.*, vol. **AE-15**, 613–619.

[16] ___, 1980: Spectral statistics for complex colored discrete-time sequences. *IEEE Trans. Acoust. Speech, and Signal Processing*, vol. **ASSP-28**, 596–599.

[17] Torres, S., C. Curtis, D. Zrnic, and M. Jain, 2007: Analysis of the new NEXRAD spectrum width estimator. *Proc. 33rd Conference on Radar Meteorology*, Cairns, Australia, AMS, P7.8.

[18] Meymaris, G., J. Williams, and J. Hubbert, 2009: An improved hybrid spectrum width estimator. *Proc. 34th Conf. on Radar Meteorology*, Williamsburg, VA, AMS, P5.20, 9 pp.

[19] Warde, D., and S. Torres, 2014: The autocorrelation spectral density for Doppler-weather-radar signal analysis, *IEEE Trans. Geosci. Remote Sens.*, vol. **GRS-52**, pp. 508–518.

[20] Welch, P., 1967: The use of fast Fourier transform for the estimation of power spectra: A method based on time averaging over short, modified periodograms. *IEEE Trans. Audio and Electro.*, vol. **AE-15**, 70–73.